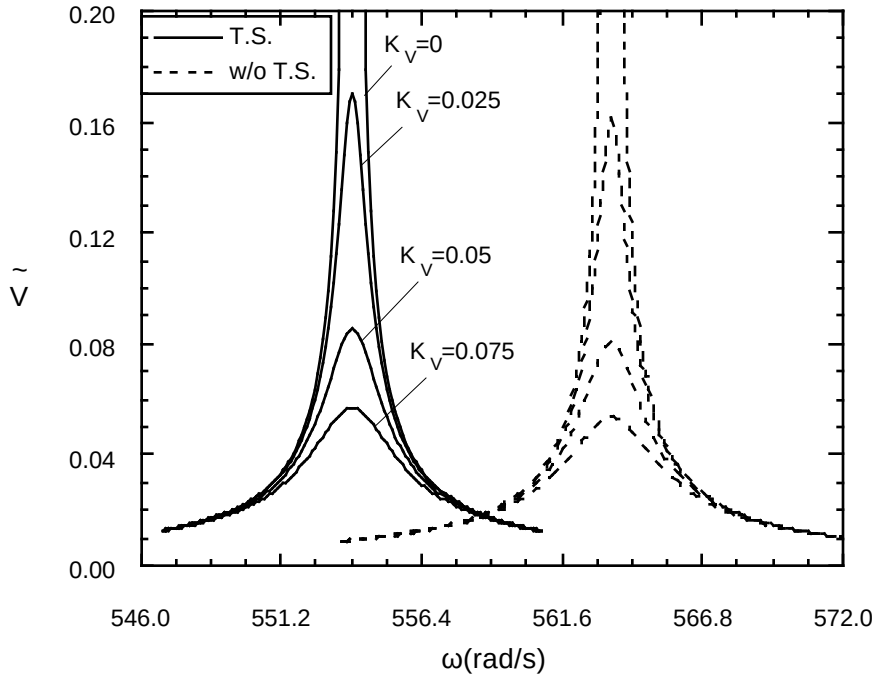

Fig. 5.1 Normalized deflection versus the excitation frequency for $AR = 6$ and $\theta = 60^{o}$ and shearable(T.S.) and nonshearable(w/o T.S.) cantilevers. Warping considered.

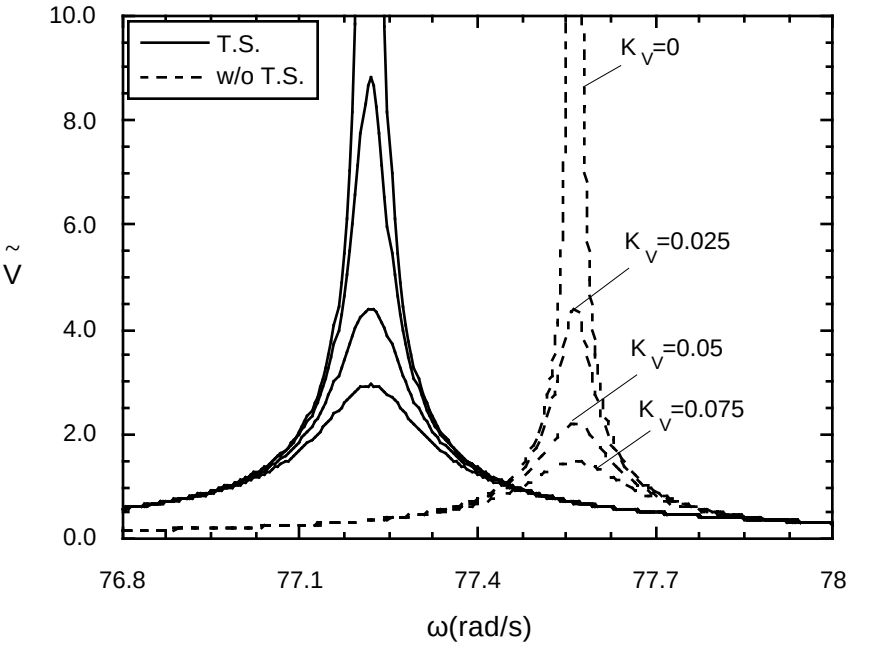

Fig. 5.2 Normalized deflection versus the excitation frequency for $AR = 16$ and $\theta = 60^{o}$ and shearable(T.S.) and nonshearable(w/o T.S.) cantilevers. No warping considered.

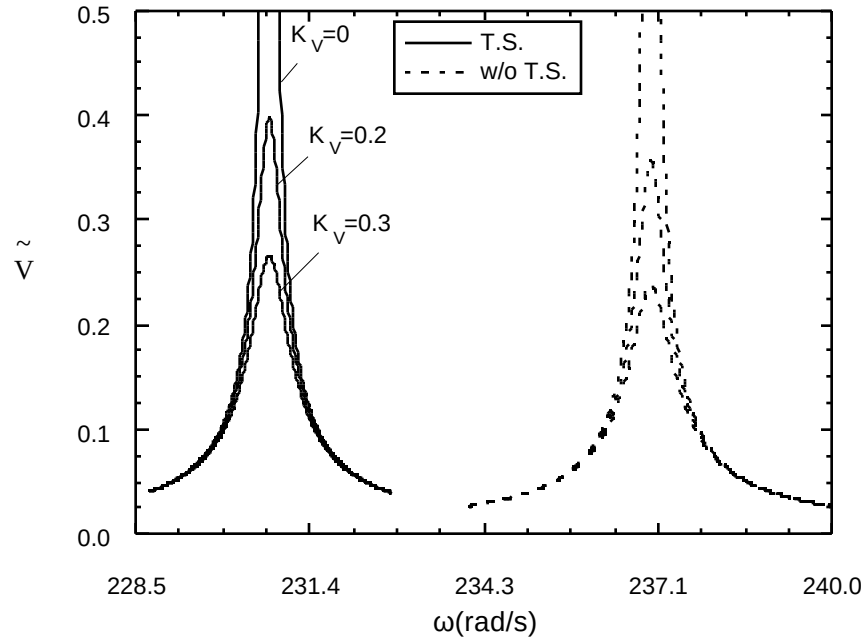

Fig. 5.3 Normalized deflection versus the excitation frequency for $AR = 16, \theta = 90^{o}$ and for shearable(T.S.) and nonshearable(w/o T.S.) cantilevers. No warping considered.

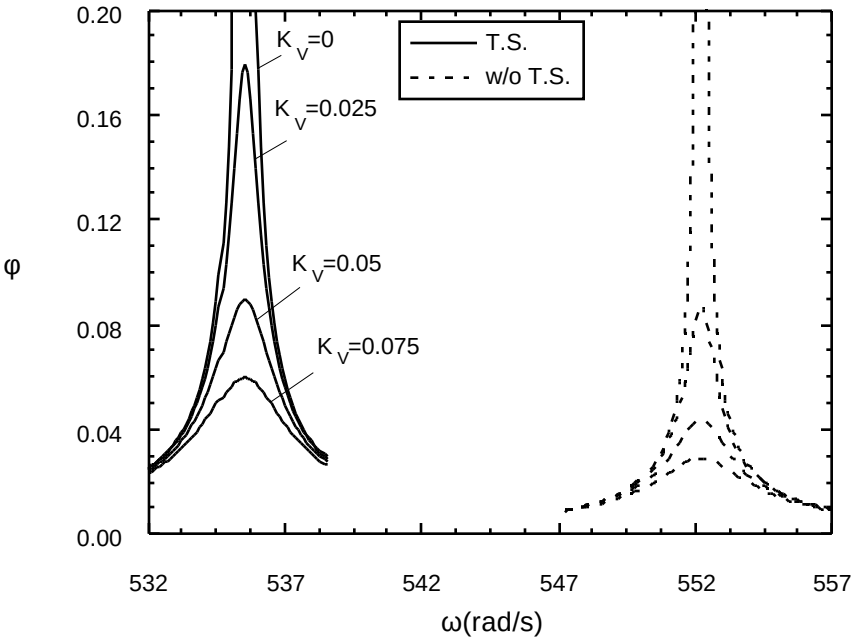

Fig. 5.4 Twist angle versus the excitation frequency for $AR = 6, \theta = 60^{o}$ and shearable(T.S.) and nonshearable(w/o T.S.) cantilevers. Free warping model considered.

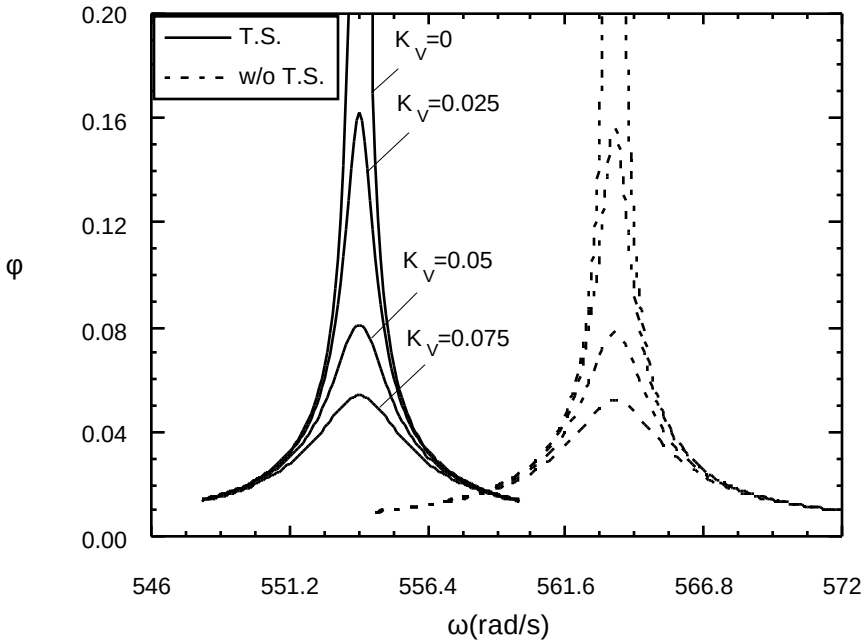

Fig. 5.5 Twist angle versus the excitation frequency for $AR = 6, \theta = 60^{o}$ and shearable(T.S.) and nonshearable(w/o T.S.) cantilevers. Warping restraint model considered.

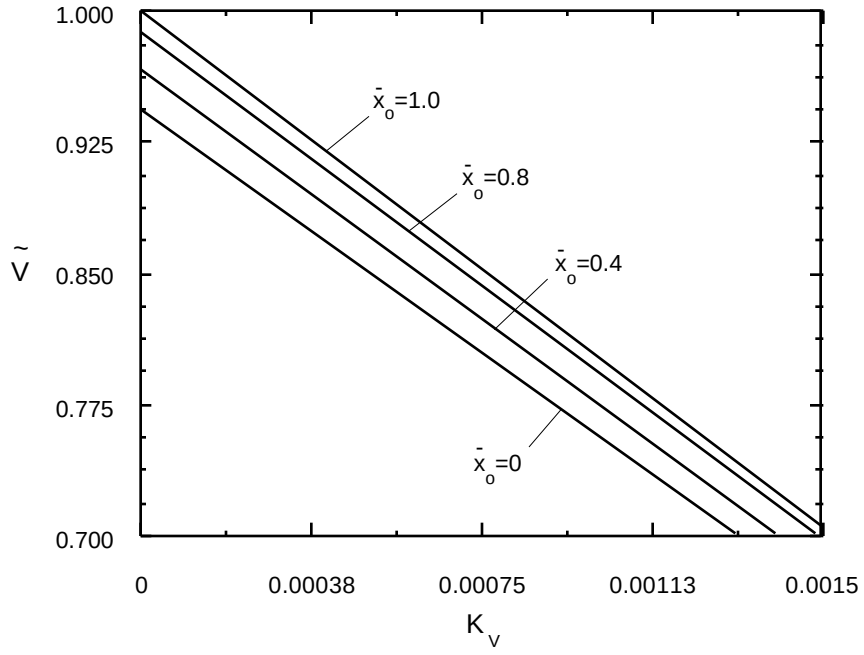

Fig. 5.6 Normalized deflection versus the feedback gain for $AR = 16, \theta = 60^{o}$.
($\tilde{V} = V/\bar{V}, \bar{V} = 2 \times 10^{5}$ corresponds to $\bar{x}_o = 1$, $K_V = 0$)

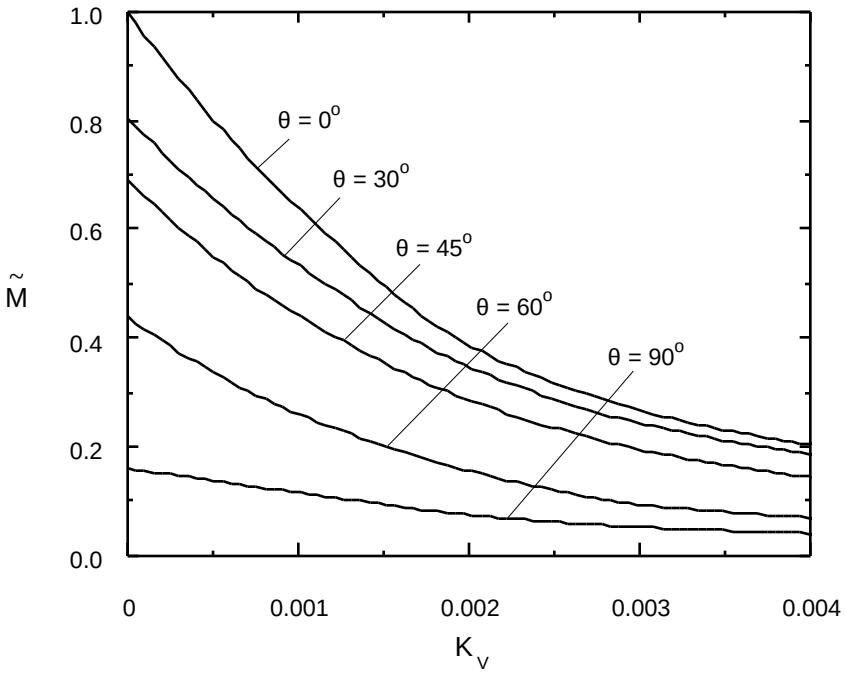

Fig. 5.7 Normalized bending moment at the wing root versus the feedback gain with the ply-angle as a parameter for $AR = 16$ ($\tilde{M} = M/\overline{M}$, $\overline{M} = 432583$ corresponds to $\theta = 0^o$, $K_V = 0$)

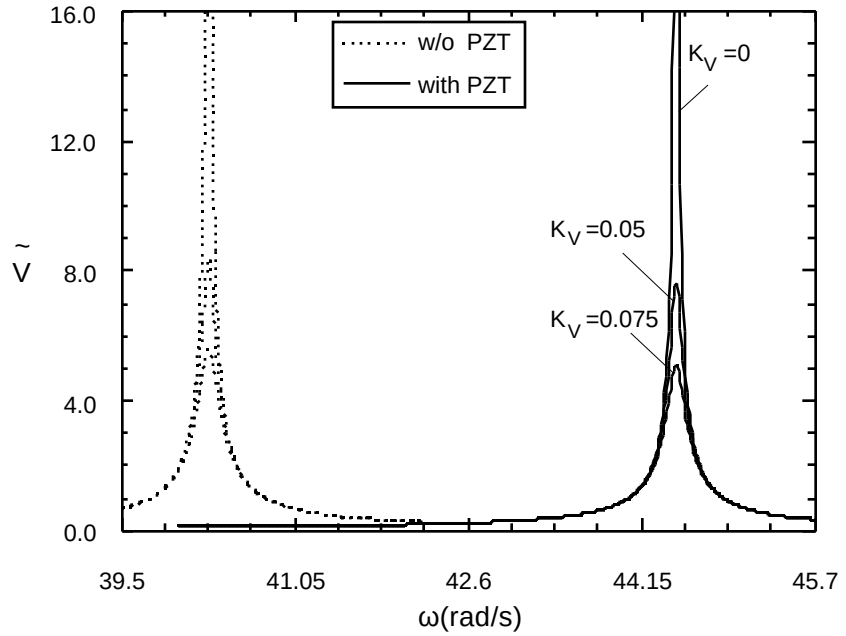

Fig. 5.8 Normalized deflection versus the excitation frequency with and without the mass and stiffness of the actuators for $AR = 16, \theta = 0^o$.

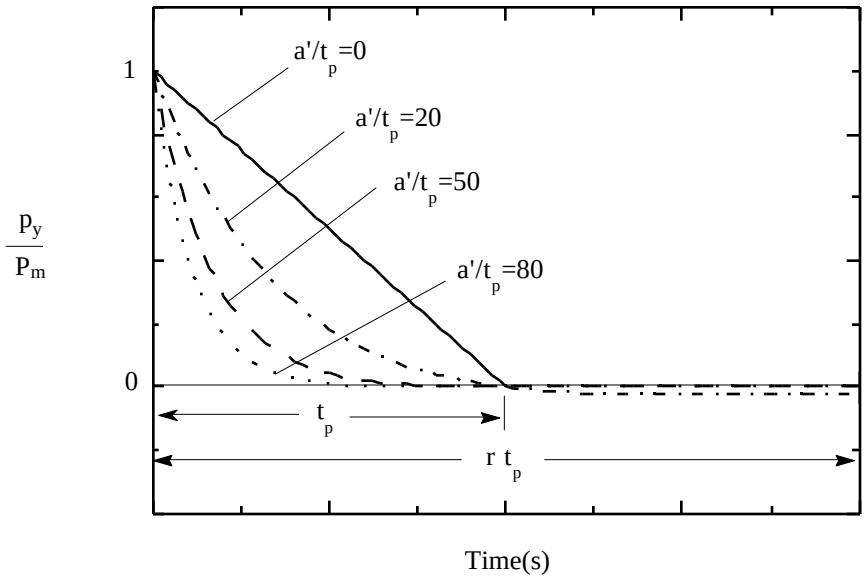

Fig. 5.9(a) Explosive overpressure signature for various values of a'/t_p .
Negative phase of the pulse included.

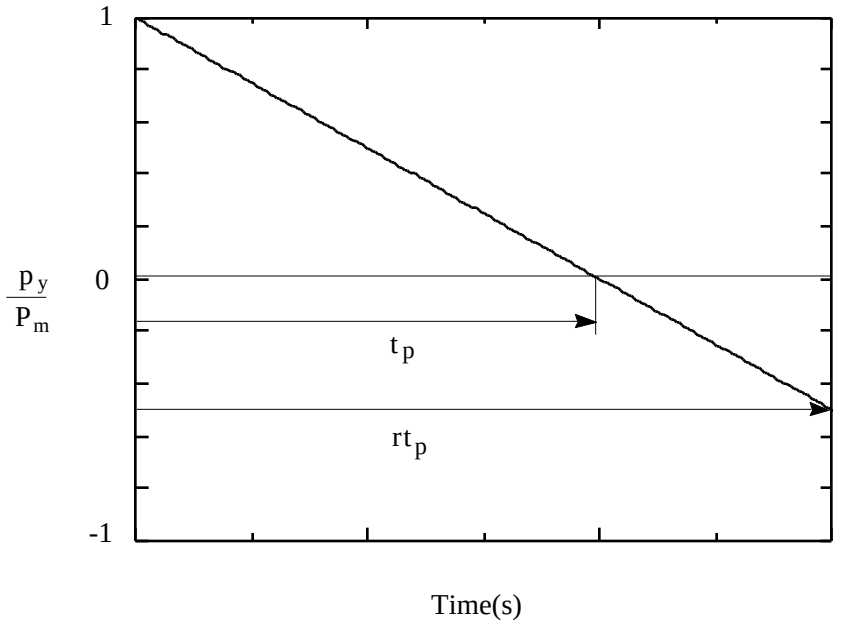

Fig. 5.9(b) Sonic-boom overpressure signature.

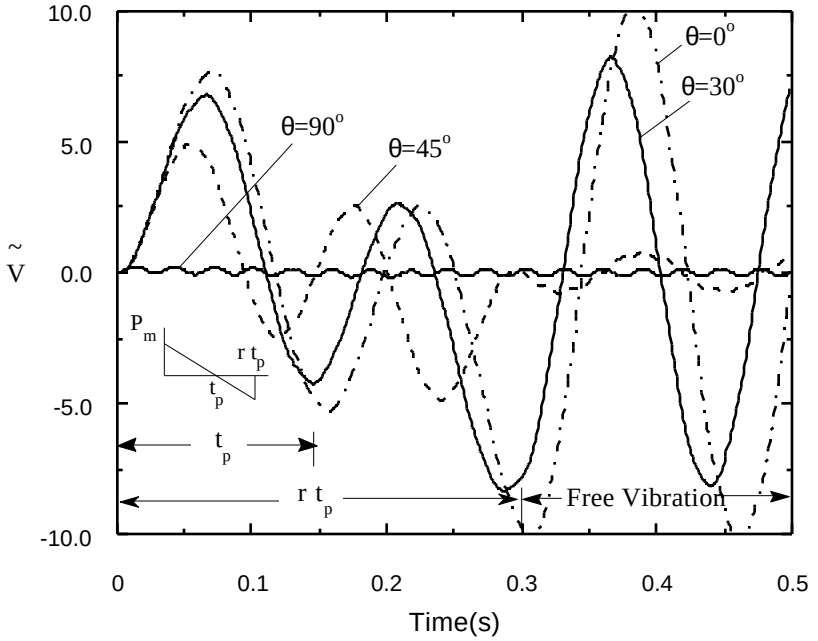

Fig. 5.10 Influence of ply-angle on time-history of the dimensionless deflection of the beam tip. Sonic-boom overpressure; $t_p = 0.15\,s, r = 1.5,$ $t_p = 0.15\,s, r = 1.5,$ Nonshearable and free-warping beam model.

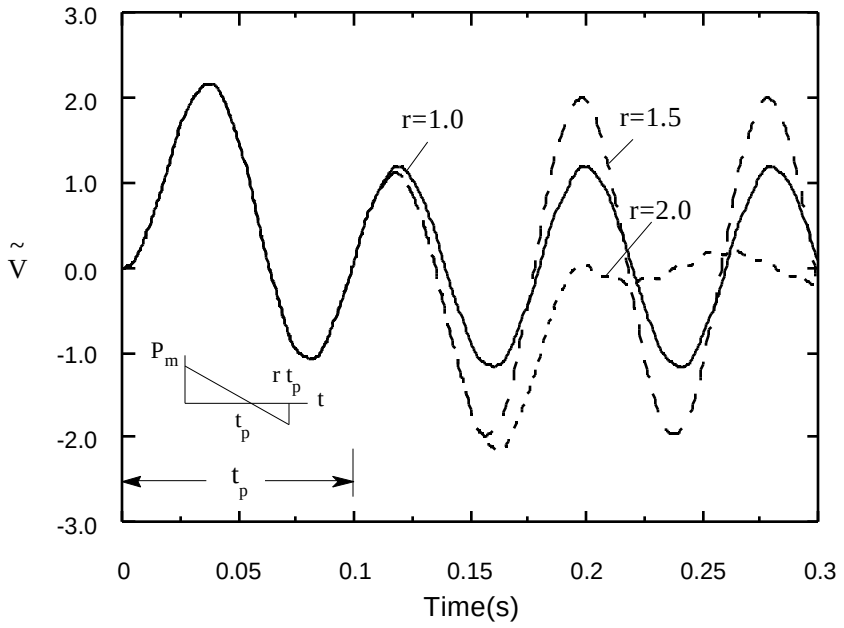

Fig. 5.11 Influence of the shock pulse length on the time-history of the dimensionless deflection of the beam tip. Sonic-boom overpressure, $t_p = 0.1\,s,$ $AR = 16, \theta = 60^{o}$, transverse shear and warping restraint included.

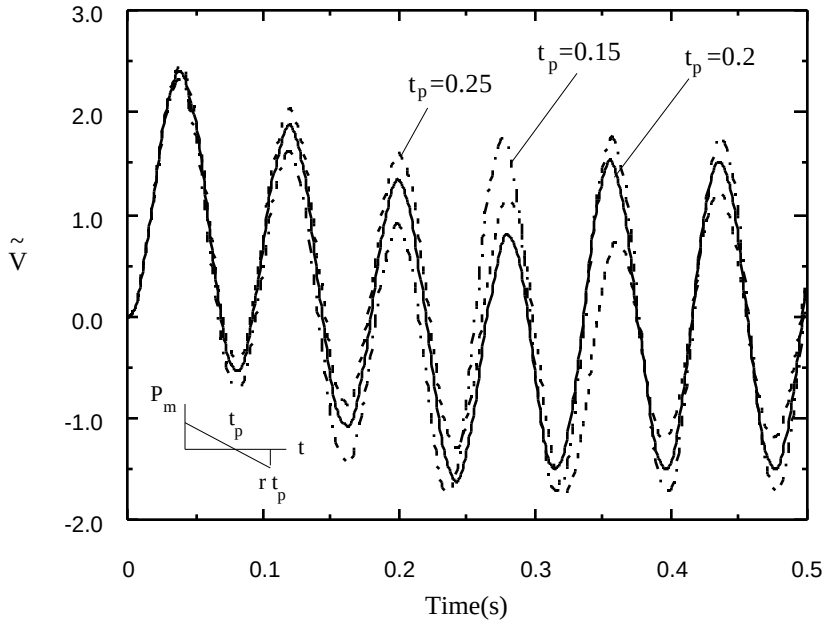

Fig. 5.12 Influence of the positive phase duration of the sonic-boom pulse on the time-history of the dimensionless deflection of the beam tip; $r = 1.5$, $AR = 16$, $\theta = 60^o$, transverse shear and warping restraint model.

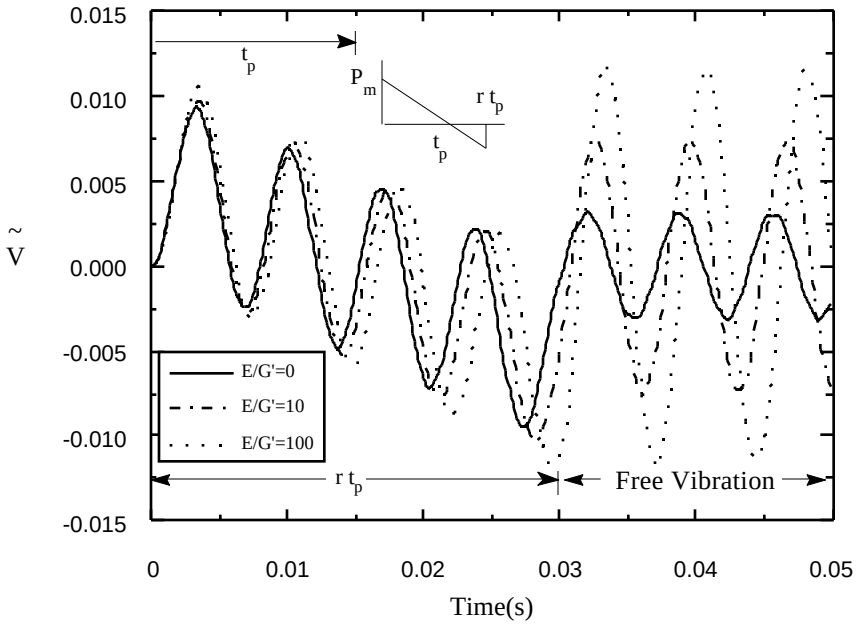

Fig. 5.13 Effect of transverse shear on time-history of the dimensionless deflection of the beam subjected to sonic-boom pulse, warping inhibition included.

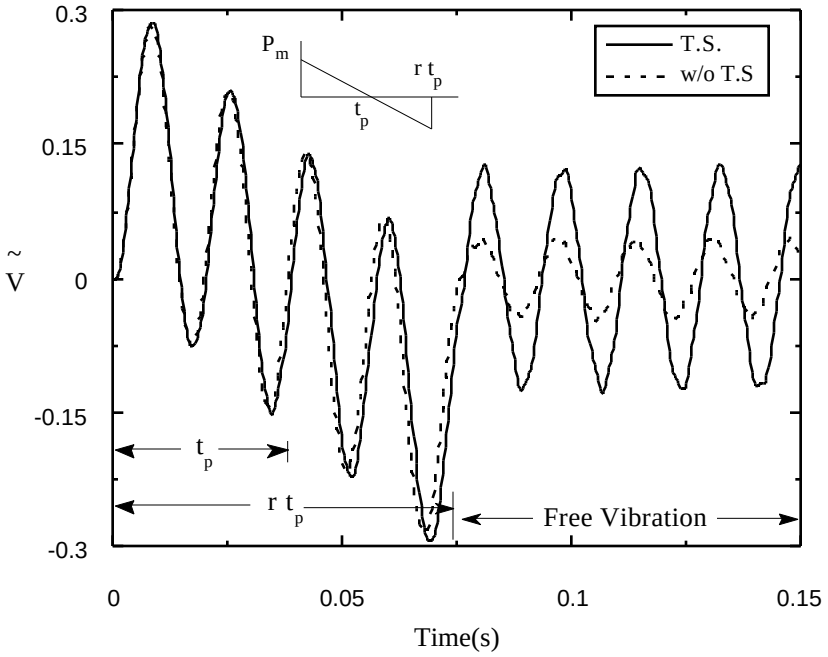

Fig.5.14 Influence of transverse shear on time-history of the dimensionless deflection of the beam tip subjected to sonic-boom pulse, $t_p = 0.037\ s, r = 2, AR = 6,$ $\theta = 45^o$, Free-warping model.

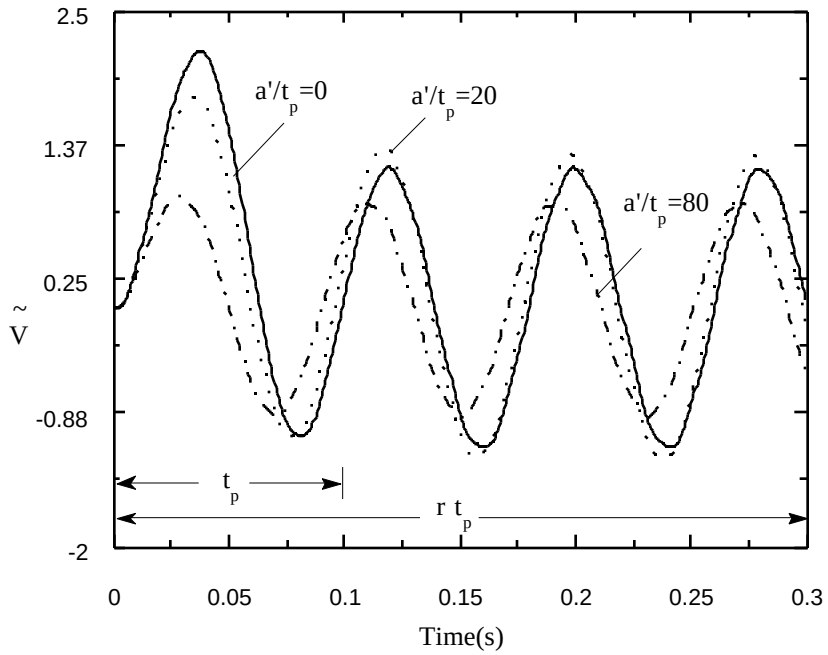

Fig.5.15 Influence of parameter a'/t_p on time-history of the dimensionless deflection of the beam tip; blast pulse, $t_p = 0.1\ s, r = 3, AR = 16,$ $\theta = 60^o$ (warping restraint model).

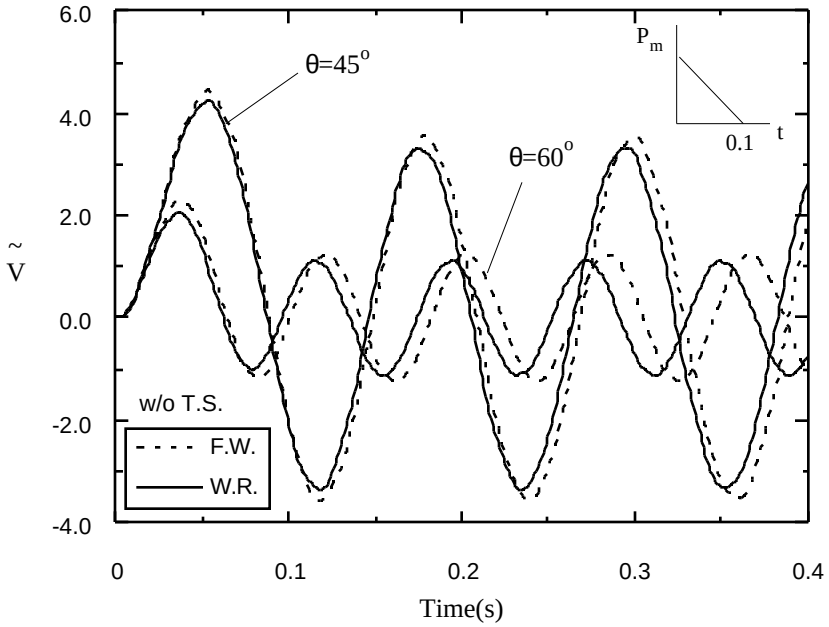

Fig. 5.16 Influence of warping restraint and of the ply-angle orientation on time-history of the dimensionless deflection of the beam tip; blast pulse, $t_p = 0.1\,s, r = 1, AR = 16$, nonshearable beam model.

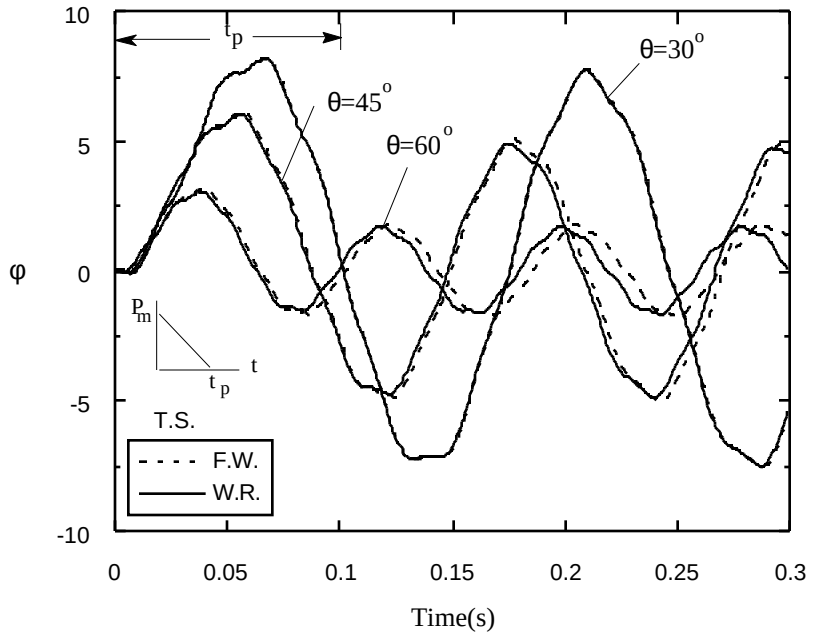

Fig. 5.17 Influence of ply-angle and warping restraint on the time-history of the twist of the beam tip; blast pulse; $t_p = 0.1s, AR = 16$ shearable beam model.

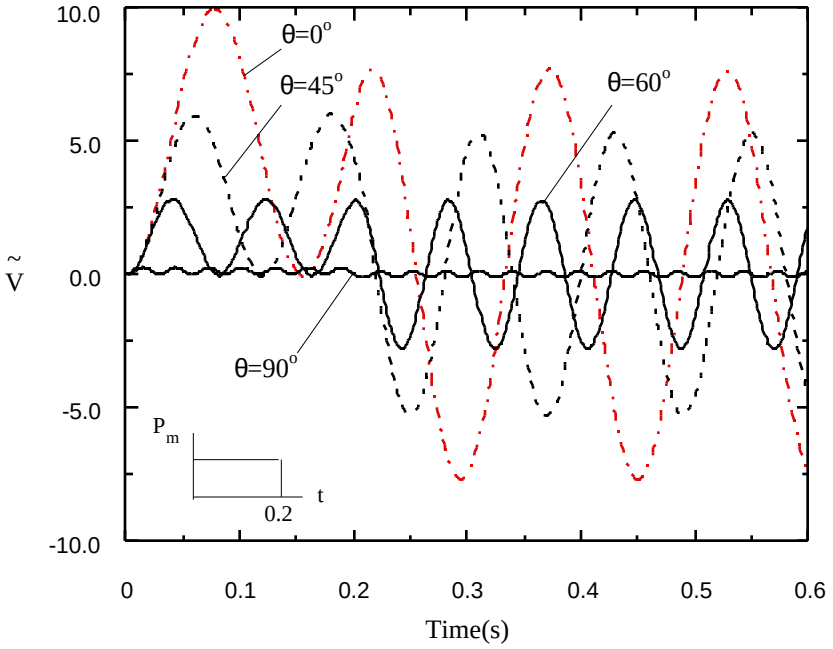

Fig. 5.18 Influence of the ply-angle on time-history of the dimensionless deflection response of the beam tip; rectangular pulse; $t_p = 0.2s$, $AR = 16$, non-shearable and free warping beam models.

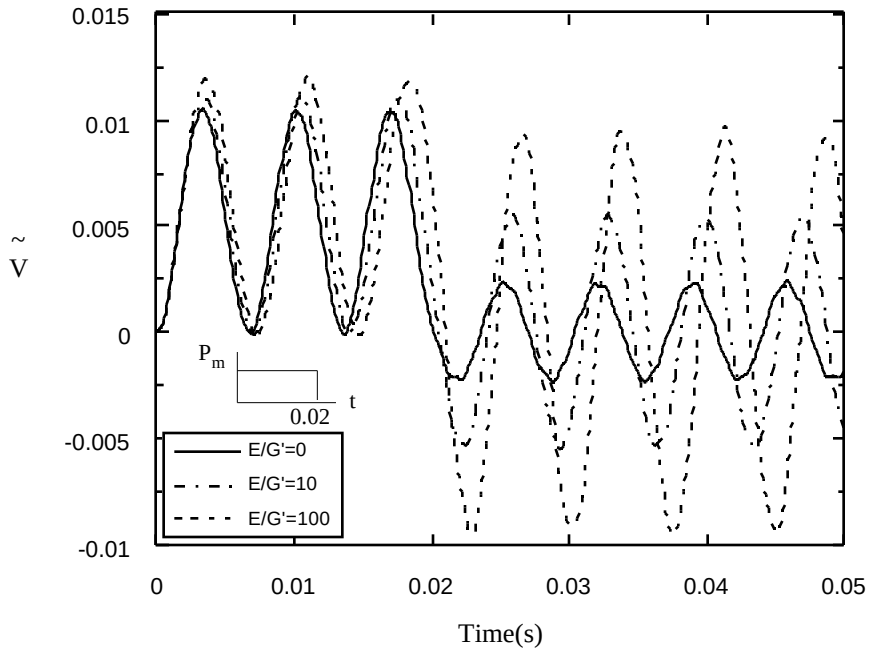

Fig. 5.19 Influence of transverse shear on time-history of the dimensionless deflection response of the beam tip; rectangular pulse; $t_p = 0.02s$, $AR = 6$, warping inhibition included.

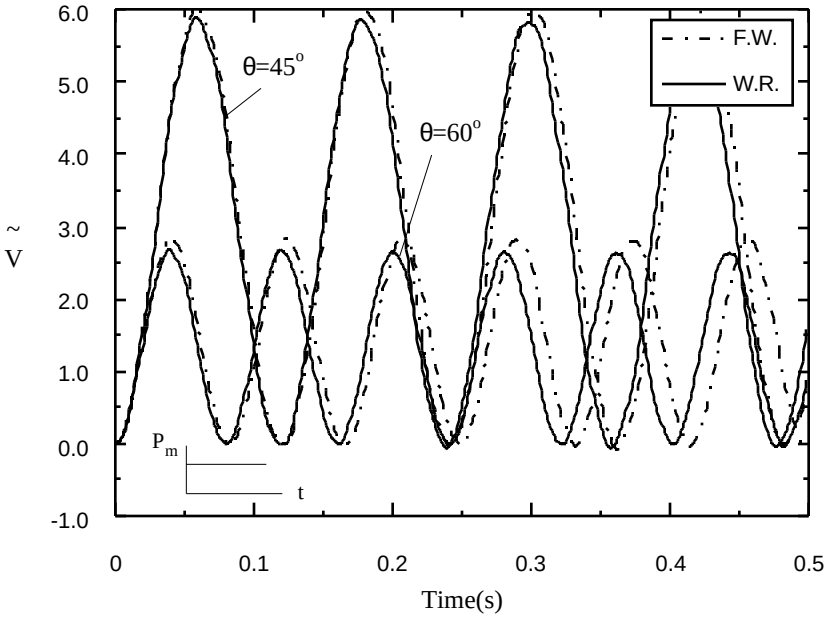

Fig. 5.20 Influence of ply-anlge on time-history of the dimensionless deflection response of the beam tip; step pulse; $AR = 16$, non-shearable beam model

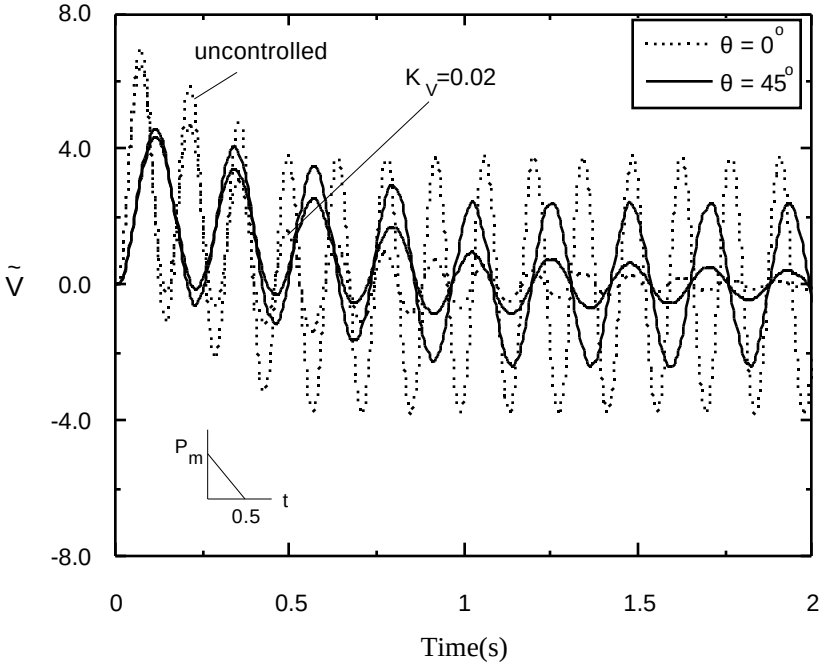

Fig. 5.21 Influence of ply-angle on open and closed-loop non-dimensional transverse deflection time-history to a blast loading; $t_p = 0.5s, AR = 16$, non-shearable and free-warping beam model.

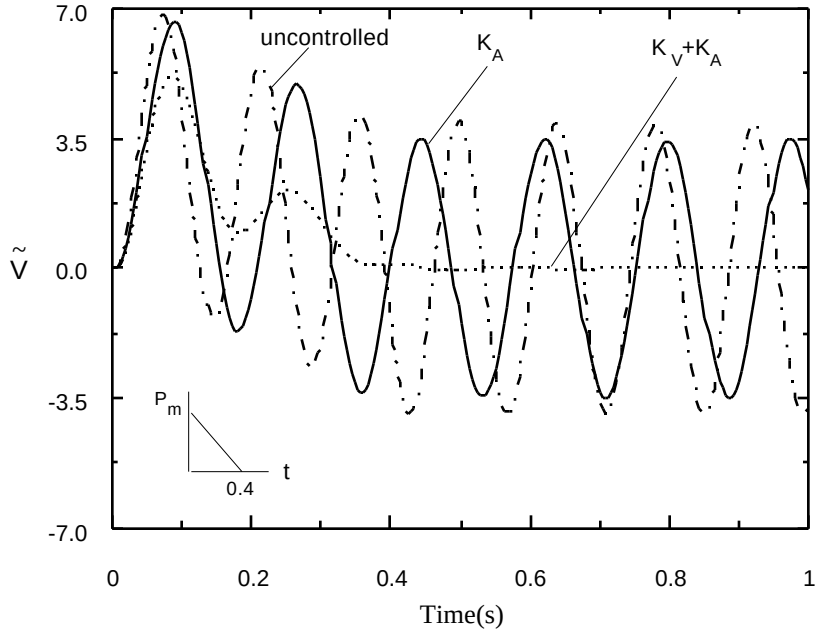

Fig. 5.22 Influence of the velocity and acceleration feedback control on the nondimensional transverse deflection time-history to a blast loading. Non-shearable and free warping beam model, $\theta = 0^o$, $AR = 16$, $K_V = 0.1, K_A = 0.005$.

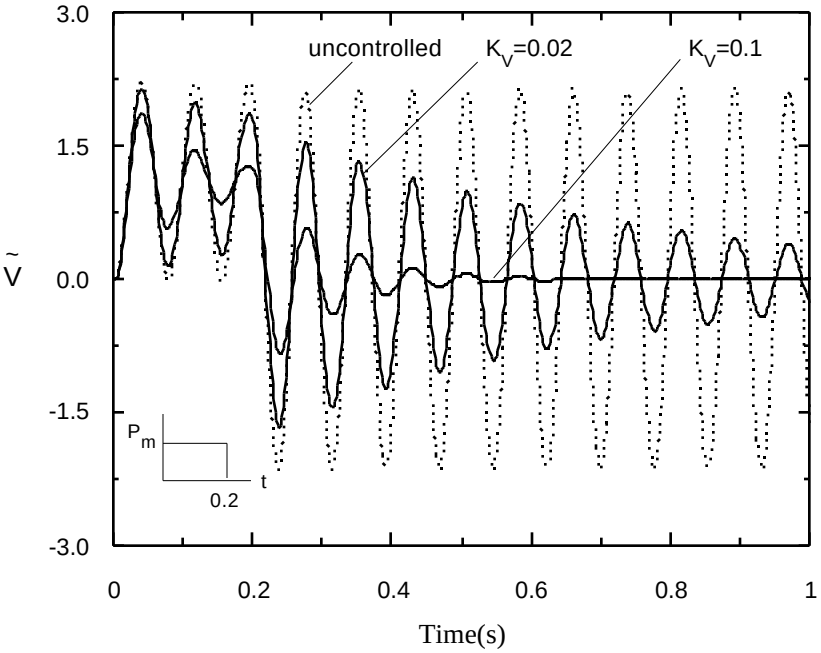

Fig. 5.23 Open and closed-loop non-dimensional transversal deflection time-history to a rectangular pressure pulse. Nonshearable and warping restraint beam model, $\theta = 0^o$, $AR = 16$.

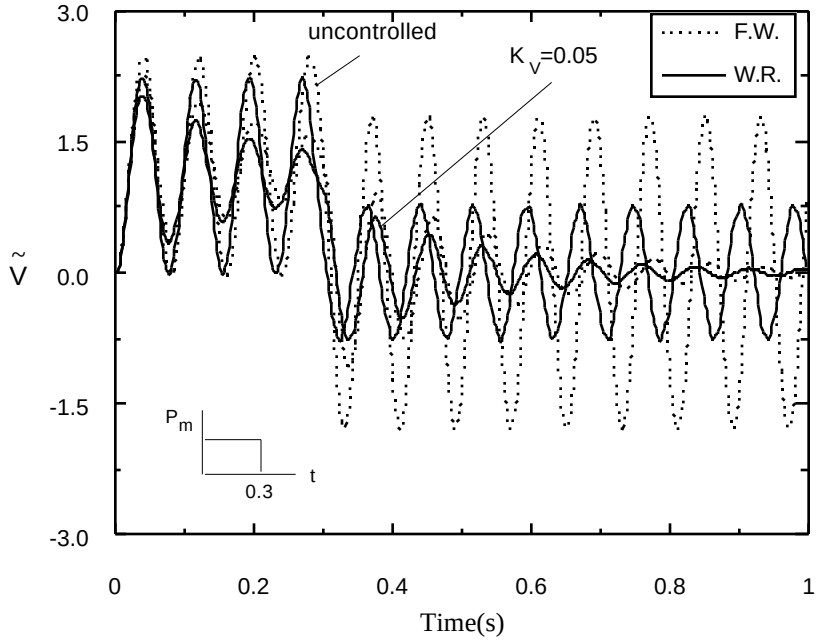

Fig. 5.24 Free and warping restraint effect on open and closed-loop transverasal deflection time-history to a rectangular pressure pulse. Non-shearable beam model; $\theta = 60^o, AR = 16$.

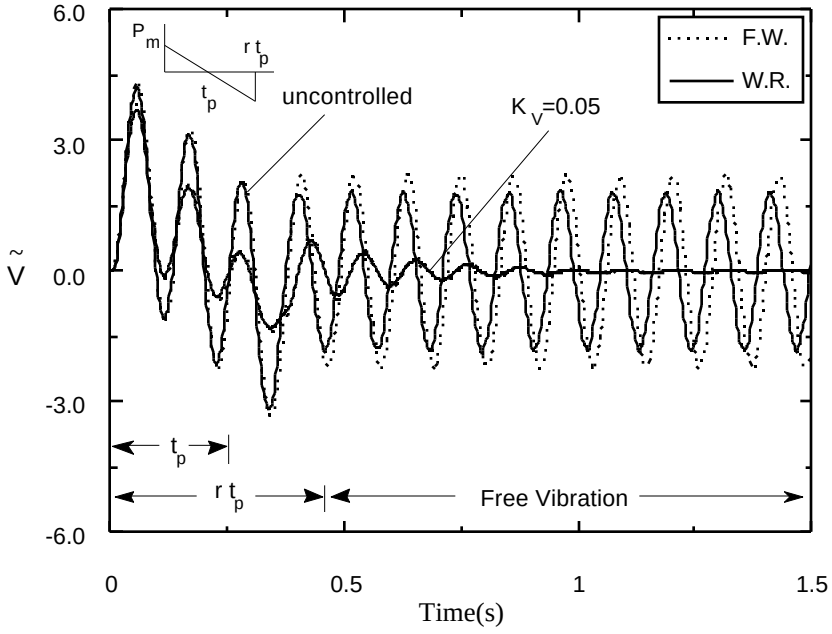

Fig. 5.25 Free and warping restraint effect on open and closed-loop transverasal deflection time-history to a sonic-boom pressure pulse. Non-shearable beam model; $\theta = 45^o, AR = 16, r = 1.5, t_p = 0.15s$.

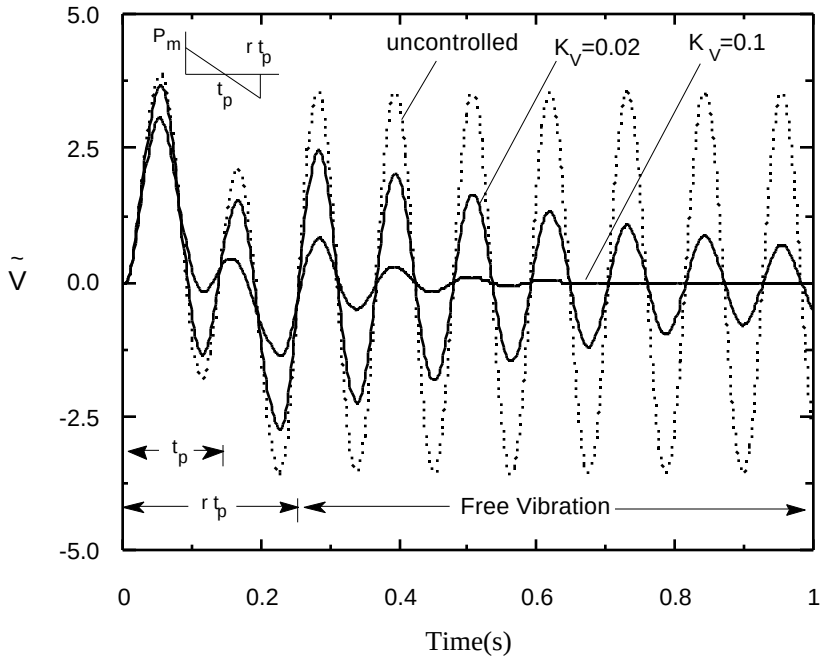

Fig. 5.26 Influence of the velocity feedback gain on the transversal deflection time-history under a sonic-boom pressure pulse. Non-shearable and warping restraint beam model; $\theta = 45^o, AR = 16, r = 1.5, t_p = 0.15s$.

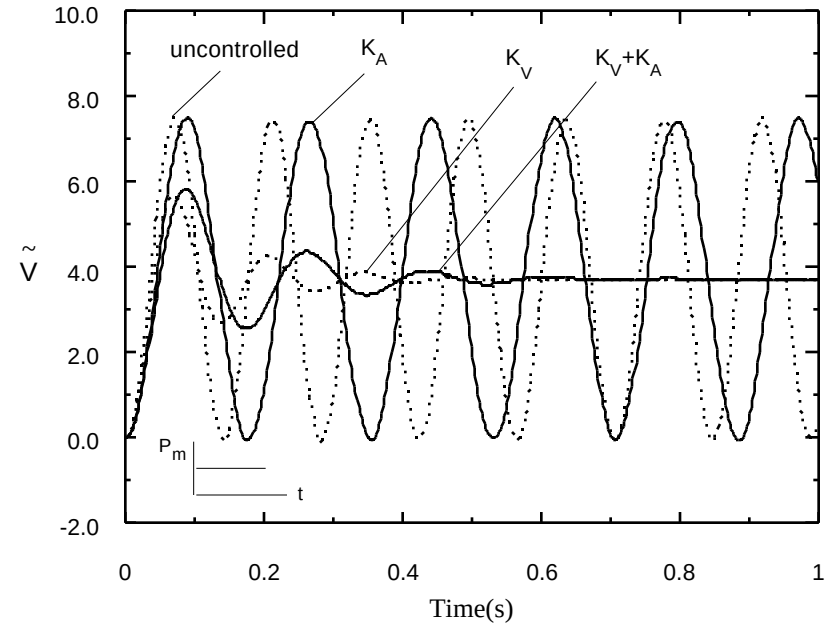

Fig. 5.27 Influence of the velocity and acceleration feedback control on the dimension-less transversal deflection time-history response to a step-pulse. Free warping and non-shearable beam model. $\theta = 0^o, AR = 16, K_V = 0.1, K_A = 0.005$.

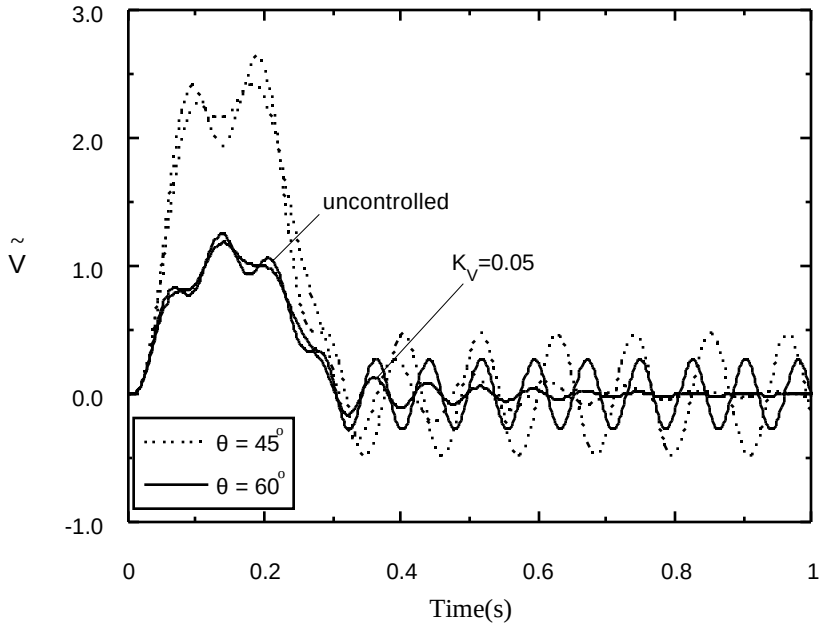

Fig. 5.28 Influence of the ply-angle and velocity feedback control upon the time-history transversal deflection to a sinusoidal pressure pulse. Non-shearable and warping restraint beam model. $AR = 16$.

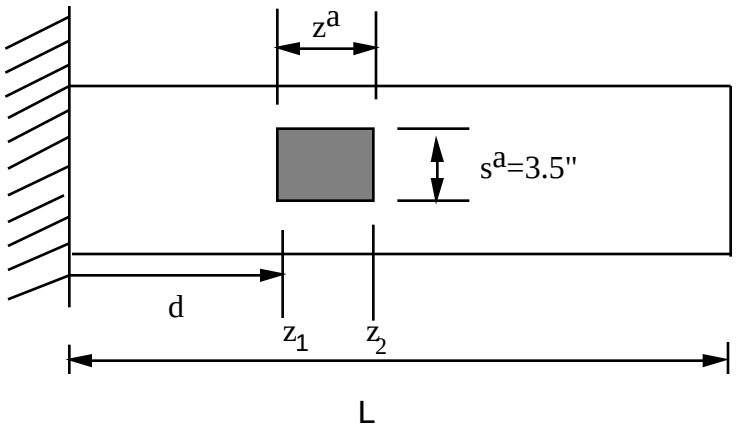

Fig. 5.29 Segmented piezoactuator configuration.
piezoactuator thickness, $t^a = 0.00787"$,
spanwise length, $L = 30"$.

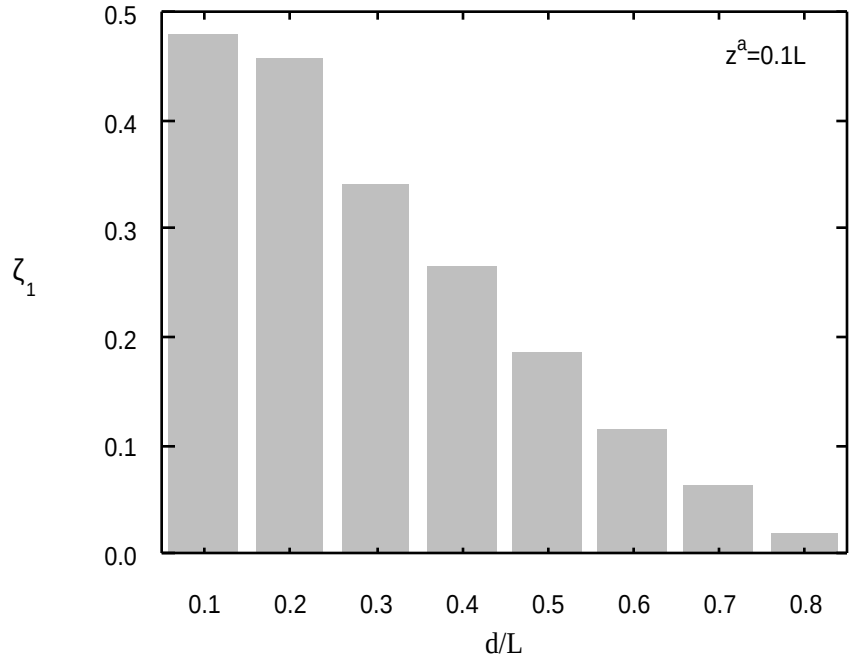

Fig. 5.30 Influence of piezoactuatore patch location on damping factor.

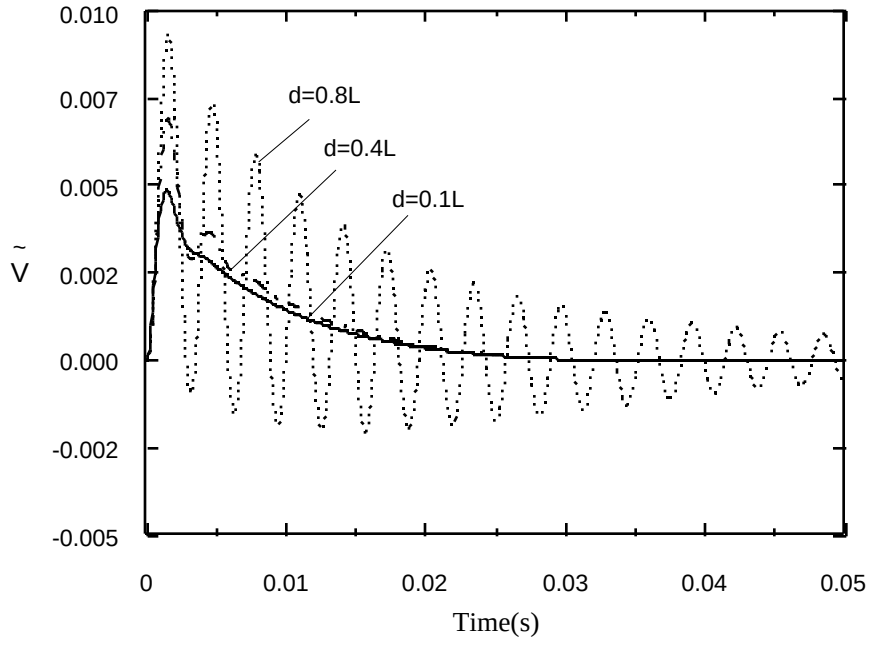

Fig. 5.31 The effects of location of piezo-patch on the beam tip deflection time history when the beam is exposed to a blast pulse.

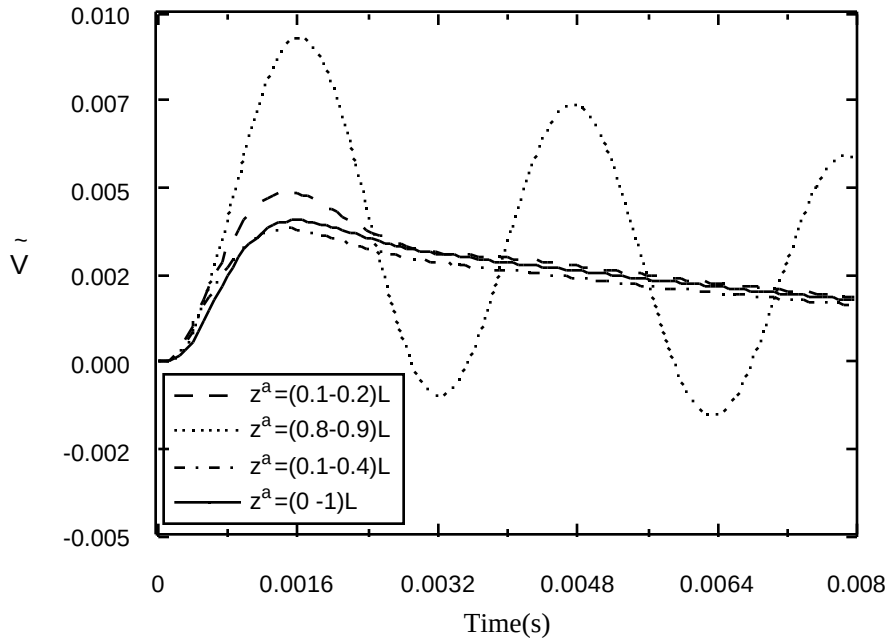

Fig. 5.32 Influence of size and location of the piezo-patch on the beam tip deflection time history when the beam is exposed to a blast load.

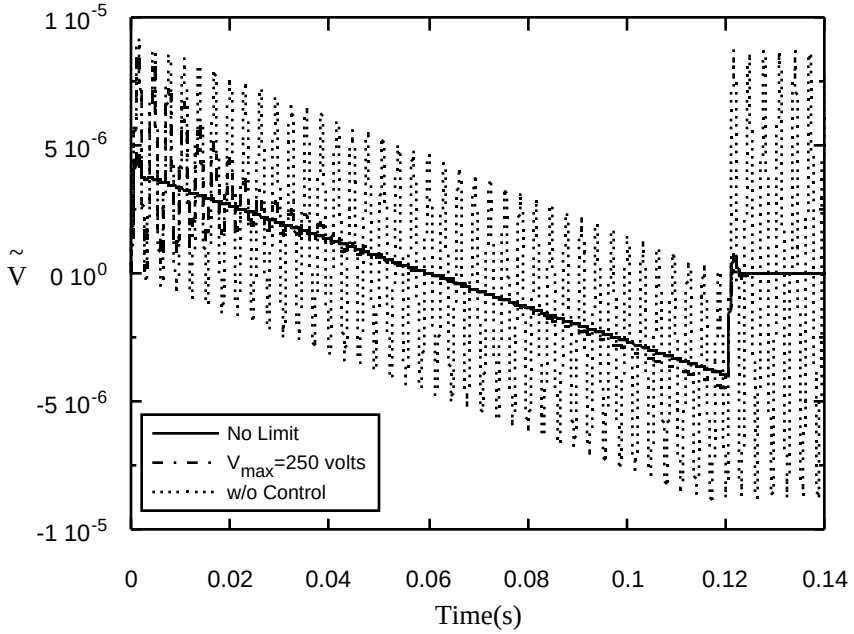

Fig. 5.33 Influence of limitation of control input voltage on transveral nondimensional deflection at the tip of the beam $z^a = (0.1 - 0.2)L$.

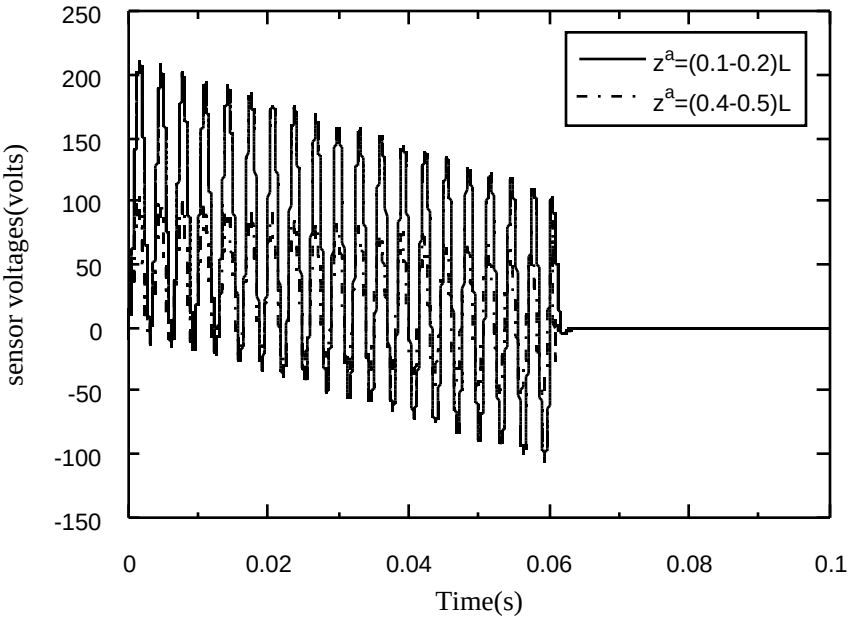

Fig. 5.34 Influence of sensor location on sensor output voltage (triangular pulse, $t_p = 0.06\text{sec}$)

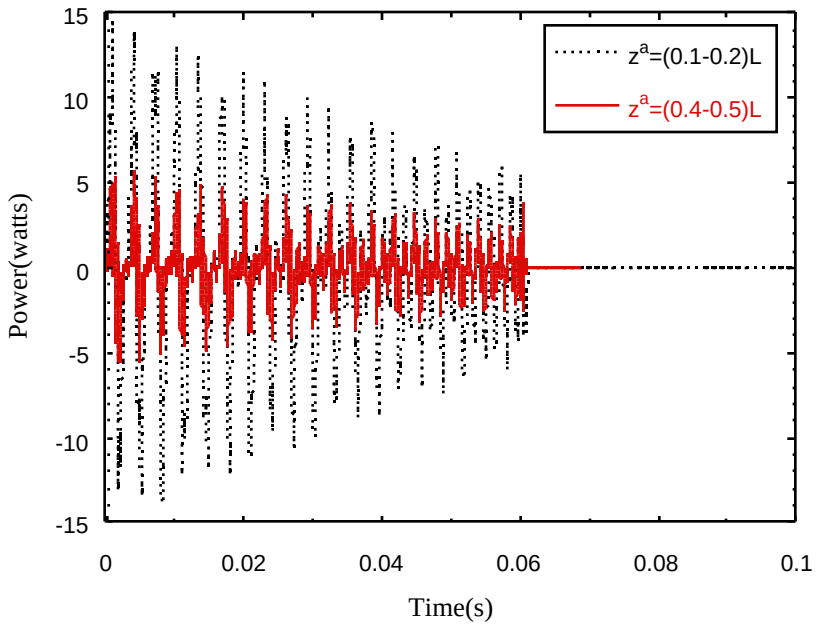

Fig. 5.35 Power consumption variation during suppression of beam vibration subjected to blast load ($P_m = 500\,\frac{lb}{L}, t_p = 0.06\text{sec}$).

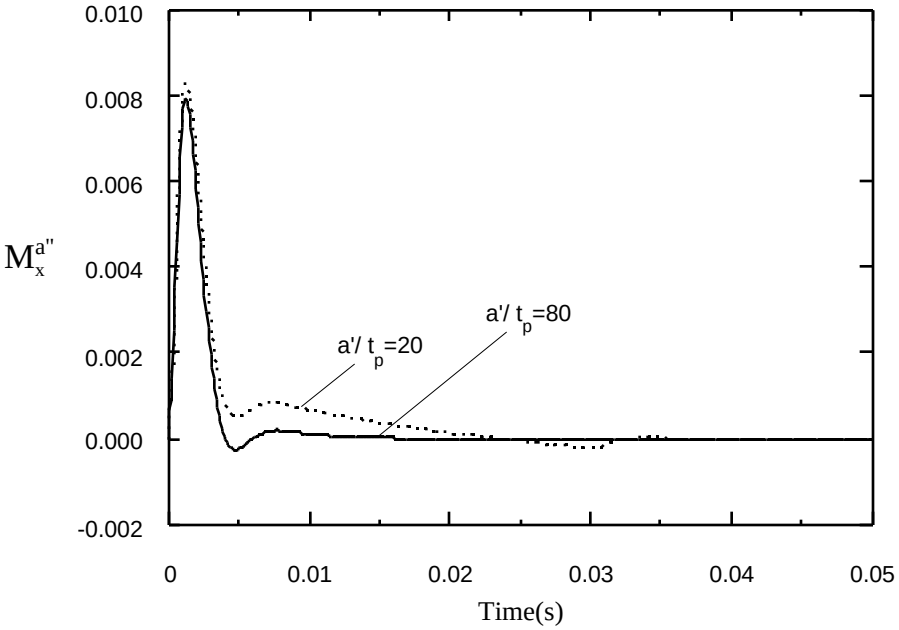

Fig. 5.36 Variation of the control force required during suppression of the beam subjected to the blast load.

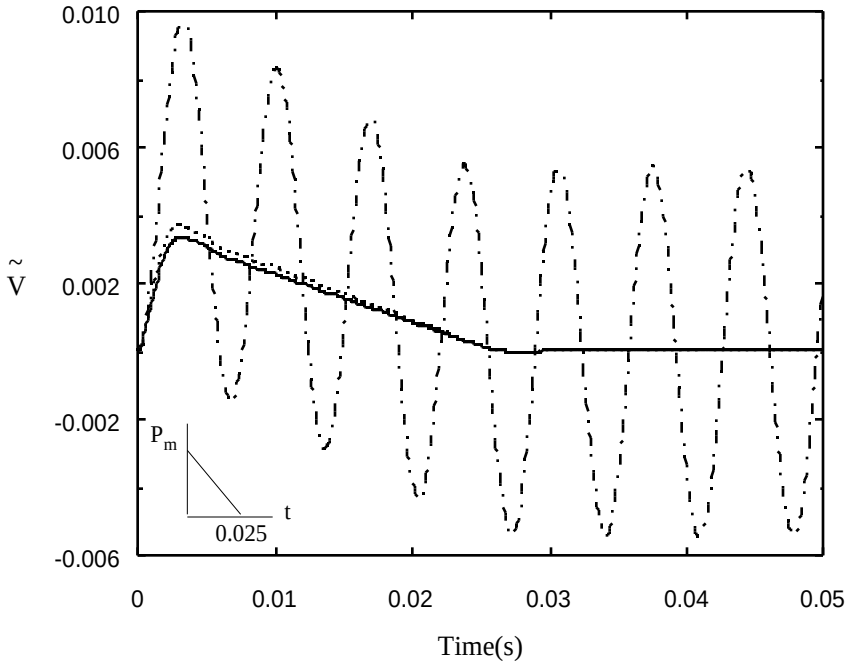

Fig. 5.37 Influence of the consideration (solid) and discard (dotted) in the performance index of external time-dependent excitation on the beam tip deflection time-history when exposed to a blast loading, AR=6; Solid-dotted line denotes uncontrolled response.

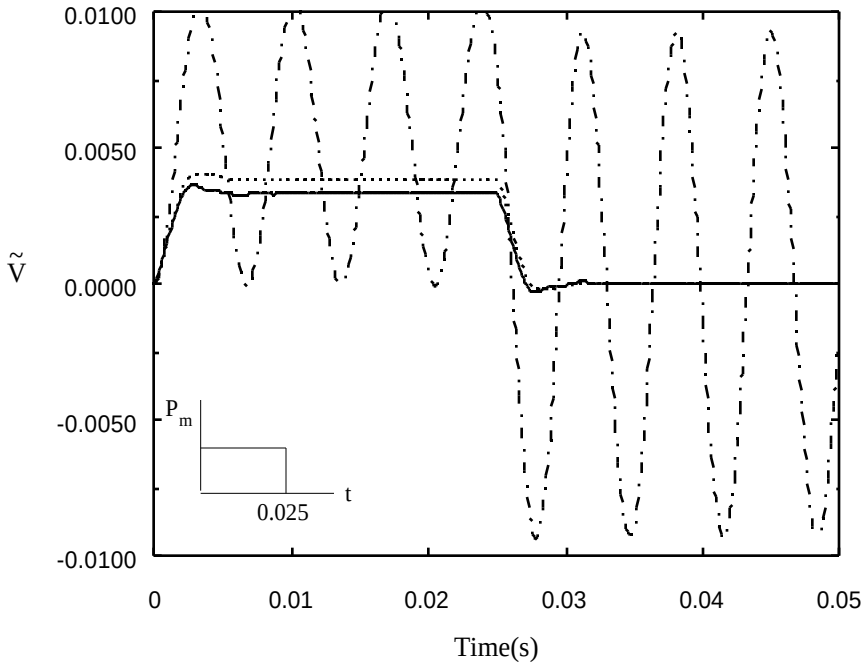

Fig. 5.38 Counterpart of Fig. 5.37 for the case of a rectangular pressure pulse.

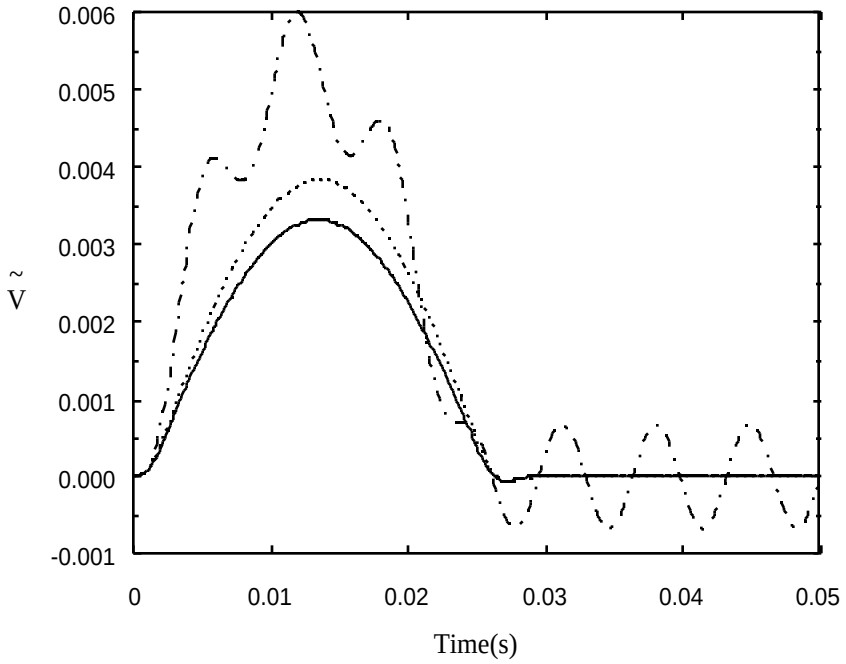

Fig. 5.39 Counterpart of a Fig. 5.37 for the case of a sinusoidal pressure pulse.